RSC Advances

PAPER

View Article Online
View Journal | View Issue

Cite this: *RSC Adv.*, 2017, **7**, 23093

$CuCo_2O_4$ nanowire arrays supported on carbon cloth as an efficient 3D binder-free electrode for non-enzymatic glucose sensing

X. Luo,[a] M. Huang,[a] L. Bie,[a] D. He,[a] Y. Zhang[b] and P. Jiang *[a]

Received 14th February 2017
Accepted 19th April 2017

DOI: 10.1039/c7ra01840a

rsc.li/rsc-advances

$CuCo_2O_4$ nanowire arrays supported on carbon cloth ($CuCo_2O_4$ NWAs/CC) were prepared *via* a simple hydrothermal synthesis and subsequent calcination process. As a 3D binder-free electrode for non-enzymatic glucose sensing, $CuCo_2O_4$ NWAs/CC shows high sensing performance towards glucose under alkaline conditions, with a wide detection range from 1 μM to 0.93 mM, a low detection limit of 0.5 μM (S/N = 3), and a high detection sensitivity of 3.93 mA mM^{-1} cm^{-2}. Moreover, $CuCo_2O_4$ NWAs/CC shows good selectivity in the presence of common interferents and good reproducibility for glucose detection, which make it a promising electrode material for sensitive determination of glucose in human samples.

Introduction

It is of great demand to have a reliable method to detect glucose in a variety of fields ranging from biomedical applications to ecological approaches.[1–3] Despite the high sensitivity and selectivity of electrochemical enzymatic glucose sensors, these sensors often suffer from the high cost of the enzyme, tedious enzyme immobilization, and the inherent instability of enzymes.[4] Therefore, it is highly attractive to develop electrochemical non-enzymatic glucose sensors.

Metals such as gold,[5,6] platinum,[7,8] palladium,[9,10] copper,[11,12] cobalt,[13,14] nickel[15,16] and their metal alloys[17,18] have been widely investigated and exploited for non-enzymatic glucose sensing. It should be noted that noble metals and their alloys exhibit high catalytic activity towards glucose oxidation, but their high cost and low availability limit their large-scale application. As such, it is highly desirable to develop inexpensive and earth-abundant 3d transition metal based electrode materials for electrochemical glucose sensing. Transition metals such as copper,[11,12] cobalt,[13,14] and nickel[15,16] have served as effective electrode materials for fabrication of non-enzymatic electrochemical glucose sensors with high sensitivity and selectivity.

Copper oxide[19,20] and cobalt oxide[13,21] have attracted more attention for non-enzymatic glucose sensing because of their simple synthesis process, super electrochemical property and good chemical stability. Their mixed metal oxide $CuCo_2O_4$, obtained from replacing Co^{2+} in $Co^{2+}(Co_2)^{3+}O_4$ spinel structure with Cu^{2+}, exhibits higher electrical conductivity and electrochemical activity than their monometallic oxides.[11,22] Consequently, $CuCo_2O_4$ shows enhanced electrochemical performance in Li-ion batteries, supercapacitors[11,23] and water splitting.[22] Because of the complex chemical compositions and the synergetic effect of both individual components, $CuCo_2O_4$ should be expected as a promising material for glucose sensing with improved performance. Indeed, the most recent reports[11,23] have demonstrated successfully the use of $CuCo_2O_4$ nanosheets grown on graphite paper and on indium doped tin oxide (ITO) coated glass substrates as non-enzymatic glucose sensor, with the detection sensitivity of 3.625 and 8.25 μA μM^{-1} cm^{-2}, respectively. $CuCo_2O_4$ nanowire arrays, which are uniformly grown on a conductive substrate, are known to be beneficial for the electronic conduction along the axial direction[24–27] from the arrays to their substrate. However, its application towards electrochemical glucose detection has not been explored before.

Here, we prepared $CuCo_2O_4$ nanowire arrays supported on carbon cloth ($CuCo_2O_4$ NWAs/CC) *via* simple hydrothermal synthesis and subsequent calcination process, and used it as a kind of binder-free electrode for non-enzymatic glucose sensing. The present sensor displays high performance with a wide linear range, a high detection sensitivity and a good selectivity against normal interferences. The excellent performance of $CuCo_2O_4$ NWAs/CC should be attributed to the following reasons: (1) binary transition metal composition of $CuCo_2O_4$ endows it improved electrochemical properties due to the synergetic effect. (2) 3D nanowire array construction not only facilitates electron transfer, but benefit for more active site exposure.[28,29] (3) The fabrication of binder-free electrode by directly grow $CuCo_2O_4$ NWAs on CC surface avoids the use of polymer binder (Nafion or PTFE) as a film-forming agent in the course of active phase immobilization on electrode surfaces, which benefits for more active site exposure and reduces the

[a]*Key Laboratory of Inorganic Functional Materials, College of Chemistry, Chongqing Normal University, Chongqing 401331, China. E-mail: jphdp868@126.com*
[b]*College of Chemistry and Materials Science, Sichuan Normal University, Chengdu 610068, China*

series resistance of the device,[30] leading to the enhanced activity.[31,32]

Experimental section

Materials

CC was purchased from Cetech Co. Ltd. (Taiwan, China). Ethanol, acetone, urea, $CoCl_2 \cdot 6H_2O$, $CuCl_2 \cdot 2H_2O$, and NaOH were purchased from Chengdu Chemical Reagent Factory (Chengdu, China). Ascorbic acid (AA), uric acid (UA), dopamine (DA) and D-(+)-glucose were supplied by J&k Chemical Ltd. (China). Human serum samples were friendly supplied by Chongqing Emergency Medical Central. All aqueous solutions were prepared with deionized water.

Preparation of $CuCo_2O_4$ NWAs/CC

Prior to hydrothermal synthesis, a piece of carbon cloth (2.5 cm × 2 cm) was cleaned by sonication sequentially in acetone, water, and ethanol for 10 min, respectively. In a typical procedure, 2.0 mmol $CoCl_2 \cdot 6H_2O$, 1.0 mmol $CuCl_2 \cdot 2H_2O$, and 9.0 mmol urea were dissolved in 15 mL water under vigorous stirring for 10 min. Then the solution was transferred into a Teflon-lined stainless autoclave and the cleaned CC was immersed into the solution. The autoclave was sealed and maintained at 120 °C for 6 h in an electric oven. After the autoclave cooled down slowly at room temperature, the precursor was taken out and washed with water and absolute alcohol thoroughly and dried in air. To prepare $CuCo_2O_4$ NWAs/CC, the obtained precursor was annealed at 300 °C for 2 h in flowing nitrogen and then cooled to ambient temperature.

Preparation of CuO and Co_3O_4 nanostructures grown on CC

For comparision, single component of metal oxide nanostructure grown on CC was prepared with the same synthesis process as that of $CuCo_2O_4$ NWAs/CC except single $CuCl_2 \cdot 2H_2O$ or 3.0 mmol $CoCl_2 \cdot 6H_2O$ was dissolved in urea solution. That is to say, 3.0 mmol $CuCl_2 \cdot 2H_2O$ or 3.0 mmol $CoCl_2 \cdot 6H_2O$ was dissolved in urea solution to prepare CuO or Co_3O_4 nanostructures grown on CC, respectively.

Characterizations

Powder XRD data were acquired on a RigakuD/MAX 2550 diffractometer with Cu Kα radiation (λ = 1.5418 Å). SEM measurements were carried out on a XL30 ESEM FEG scanning electron microscope at an accelerating voltage of 20 kV. Transmission electron microscopy (TEM) image of $CuCo_2O_4$ NTAs were performed on a HITACHI H-8100 electron microscopy (Hitachi, Tokyo, Japan) with an accelerating voltage of 200 kV. XPS measurements were performed on an ESCALABMK II X-ray photoelectron spectrometer using Mg as the exciting source.

Electrochemical test

All electrochemical measurements were performed on a Autolab PGSTAT 302 electrochemical workstation (Metrohm Ltd, Switzerland). A typical three-electrode system was employed with a statured Ag/AgCl as reference electrode, a Pt wire as counter electrode, and the $CuCo_2O_4$ NWAs/CC (0.5 cm × 0.5 cm) as a working electrode. All electrochemical experiments were performed at room temperature and all the potentials are reported against the saturated Ag/AgCl reference electrode. For amperometric detection, all measurements were performed by applying an appropriate potential to the working electrode and allowing the transient background current to decay to a steady-state value before the addition of the analyte. The solution was stirred to provide convective transport.

Results and discussion

Scheme 1 illustrates the fabrication process of $CuCo_2O_4$ NWAs/CC and its application as non-enzymatic glucose sensor. $CuCo_2O_4$ was synthesized *via* simple hydrothermal and subsequent calcination process. The mechanism was known as the incorporation Cu^{2+} to Co^{2+} from $Co^{2+}(Co^{3+})_2O_4$ spinel structure, and the corresponding chemical reaction can be expressed as follows:[11]

$$NH_2(CO)NH_2 + 5H_2O \rightarrow 4NH_4^+ + 2OH^- + CO_3^{2-} + CO_2 \quad (1)$$

$$(Cu^{2+},Co^{2+}) + 2OH^- + 2CO_3^{2-} \rightarrow (Cu,Co)_2(CO_3)(OH)_2 \quad (2)$$

$$Cu_2(CO_3)(OH)_2 + 2Co_2(CO_3)(OH)_2 + O_2 \rightarrow 2CuCo_2O_4 + 3CO_2 + 3H_2O \quad (3)$$

Fig. 1a shows the X-ray diffraction (XRD) pattern of $CuCo_2O_4$ NWAs/CC. The diffraction peaks positioned at 19.1°, 31.4°, 36.9°, 39.0°, 45.1°, 56.0°, 59.6°, 65.7°, and 77.6° can be well identified as (111), (220), (311), (222), (400), (422), (511), (440) and (533) planes of the spinel $CuCo_2O_4$ phase (JCPDS 01-1155). The strong peaks at 26° and 43° marked with "*" are assigned to the CC substrate. This fact demonstrates the successful fabrication of $CuCo_2O_4$ grown on CC. Fig. 1b shows the low-magnification scanning electron microscopy (SEM) image of $CuCo_2O_4$ NWA/CC. As observed, the entire surface of the CC is covered uniformly by a dense packed $CuCo_2O_4$ nanowire arrays. The high-magnification SEM image (Fig. 1c and d) further reveals these nanowires with diameter about 200 nm grow vertically and bundle on CC with smooth surface. Fig. 1e shows the transmission electron microscopy (TEM) image of $CuCo_2O_4$ NW, further confirming its 1D morphology. The high-resolution (HRTEM) image of the selected area in Fig. 1e shows well-resolved lattice fringes with interplanar distances of 0.24 nm, which can be indexed to the (311) plane of $CuCo_2O_4$.

The chemical composition and their oxidation state of $CuCo_2O_4$ NWAs/CC were further analyzed by XPS measurements. The survey spectrum (Fig. 2a) shows the presence of C, Cu, Co, and O elements. Fig. 2b shows the XPS 2p spectra in the Cu(2p) regions. As shown, four peaks occur at binding energies of 934.4, 942.8, 954.2 and 962.0 eV. The peaks at 934.4 and 954.2 eV could be assigned to Cu $2p_{3/2}$ and Cu $2p_{1/2}$, while the peaks at 942.8 and 962.0 eV could be indexed to the satellite

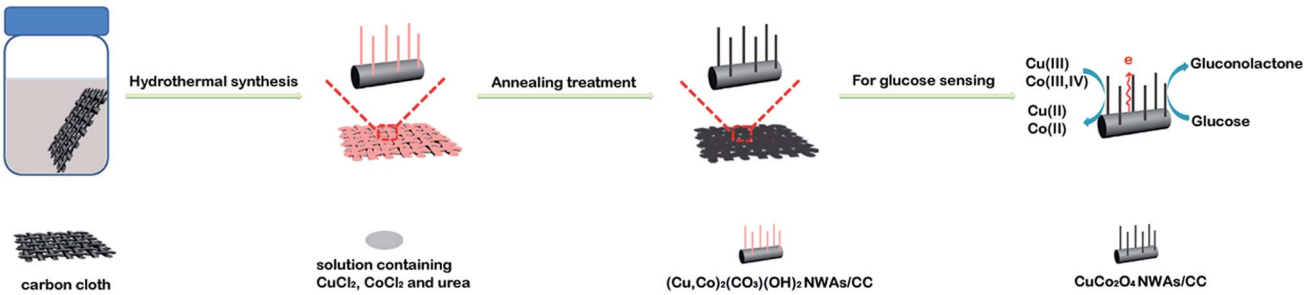

Scheme 1 The illustration of the fabrication of $CuCo_2O_4$ NWAs/CC and the possible mechanism of non-enzymatic glucose electro-oxidation on $CuCo_2O_4$ NWAs surface in alkaline medium.

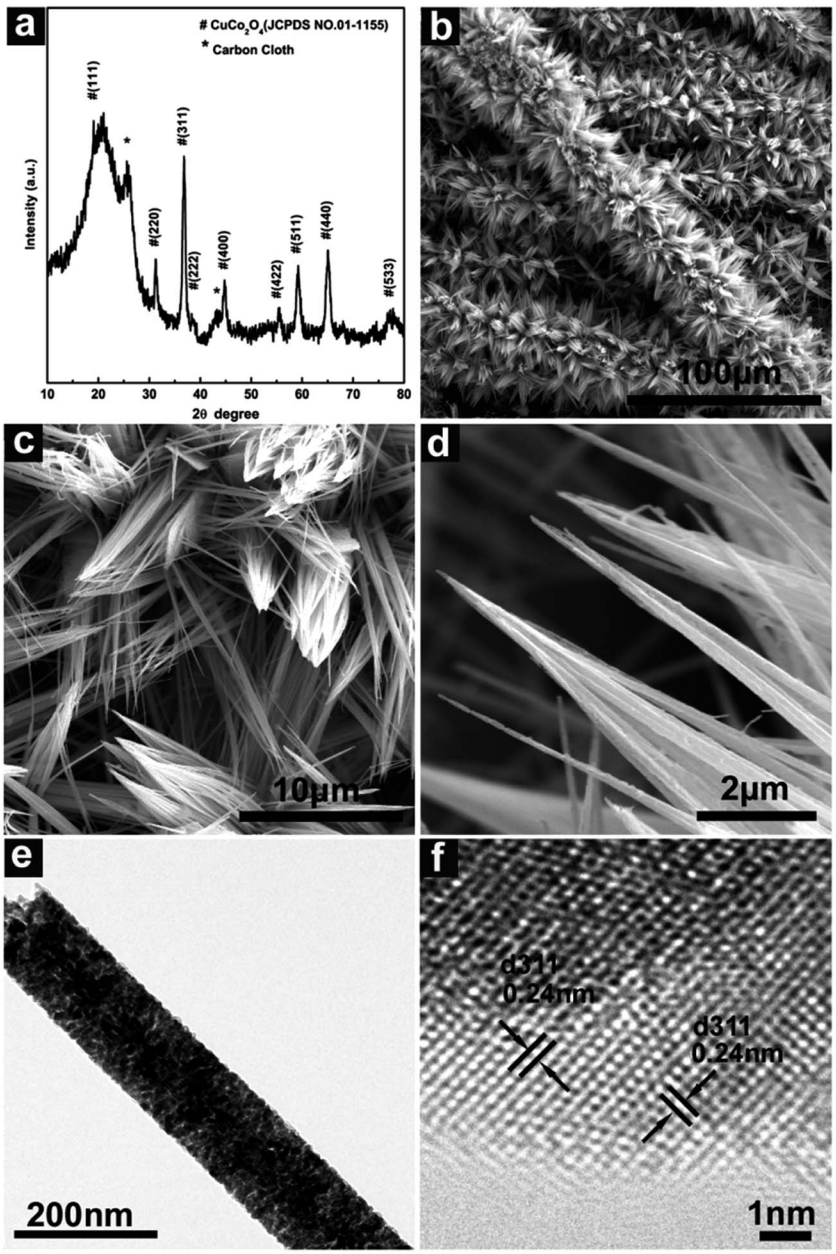

Fig. 1 (a) XRD patterns and (b–d) SEM images with different magnification of $CuCo_2O_4$ NWAs/CC. (e) TEM and (f) HRTEM images taken from one single $CuCo_2O_4$ NW.

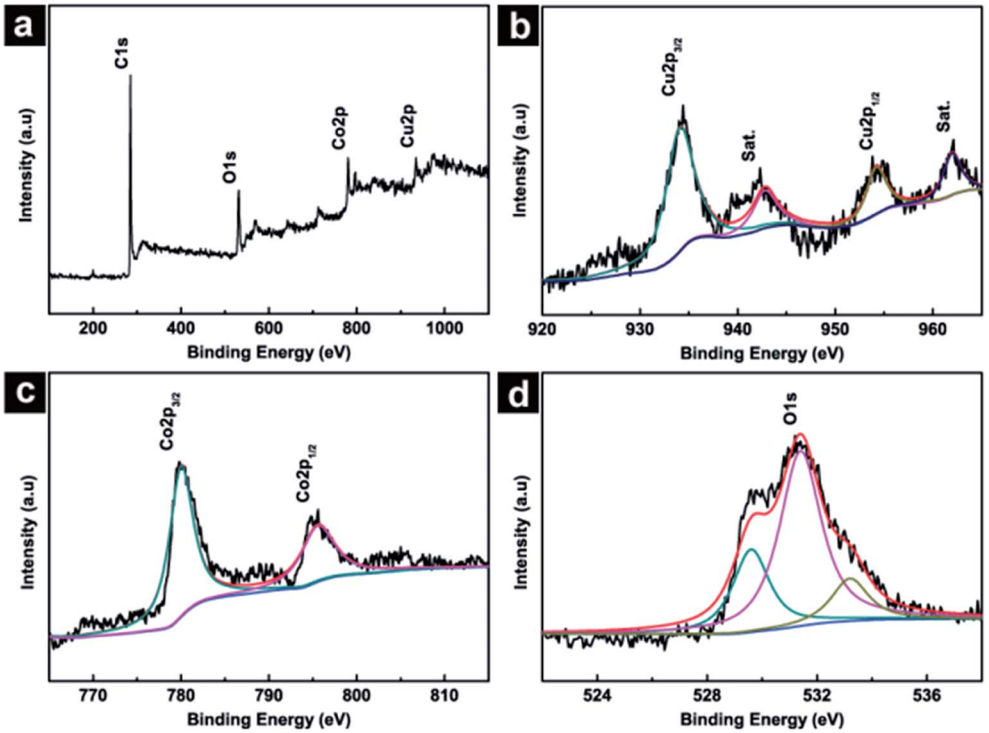

Fig. 2 XPS spectra of (a) survey scan, (b) Cu 2p, (c) Co 2p and (d) O 1s for $CuCo_2O_4$ NWAs/CC.

peaks of Cu^{2+}.[33] The Co 2p spectrum (Fig. 2c) have two peaks at binding energies of 780.0 and 795.1 eV which could be assigned to Co $2p_{3/2}$ and Co $2p_{1/2}$, suggesting the Co(III) ions in the low spin state. Fig. 2d shows the O 1s spectrum which was resolved into three components (O1, O2, and O3) with binding energies of 529.6, 531.4 and 533.2 eV. These peaks correspond to the lattice O^{2-} species, surface oxygen and absorbed oxygen species, respectively.[33] The XPS measurements support above XRD results and confirm the successfully formation of $CuCo_2O_4$ phase.

Noted that single component of metal oxide nanostructure grown on CC can be prepared under the same synthesis process. When 3.0 mmol $CuCl_2 \cdot 2H_2O$ was dissolved into urea solution and taken as precursor solution for hydrothermal synthesis followed the calcination, the product was found to be CuO. As shown in Fig. 3a, the diffraction peaks of the product was well indexed to the characteristic diffraction peaks of CuO (JCPDS 45-0937). The obtained CuO exhibits nanoparticle morphology and covers on CC (CuO NPs/CC) uniformly with the diameter around 100 nm (Fig. 3b). While 3.0 mmol $CoCl_2 \cdot 6H_2O$ dissolved and taken as precursor solution gives Co_3O_4 (JCPDS 43-1003) nanowire arrays supported on CC (Co_3O_4 NWAs/CC) (Fig. 3a and c). This fact suggests the important role of cobalt salt in the $CuCo_2O_4$ nanowire morphology formation.

$CuCo_2O_4$ NWAs/CC was directly utilized as working electrode for electrochemical test without any other pretreatment. Fig. 4a exhibits the electrochemical behavior of CC and $CuCo_2O_4$ NWAs/CC in absence and presence of 0.5 mM glucose in 0.1 M NaOH solution. Blank CC gives no redox peak in absence (blue curve) and presence (green curve) of glucose. In contrast, $CuCo_2O_4$ NWAs/CC shows two broad peaks at 0.4 V and 0.6 V in the anodic scan, and a broad peak from 0.8 V to 0.3 V in cathodic scan in absence of glucose (red curve). Like many other

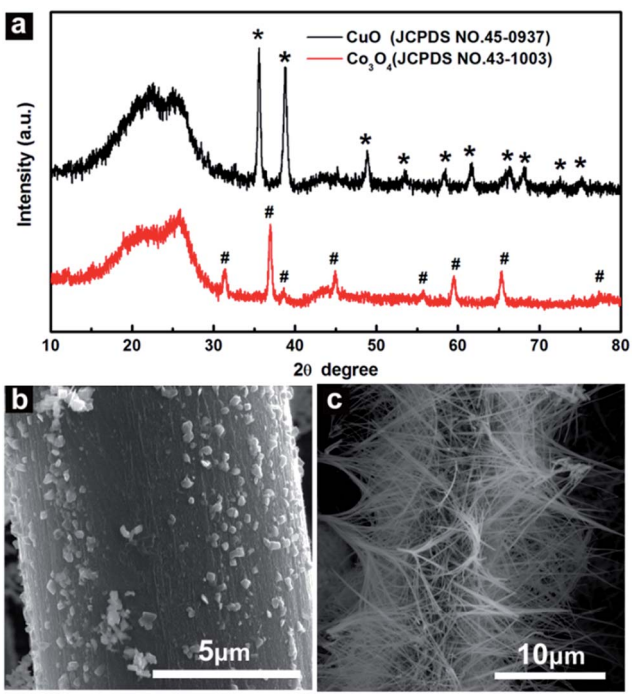

Fig. 3 (a) XRD patterns of CuO and Co_3O_4 nanostructures grown on CC. (b) SEM images of CuO and (c) Co_3O_4 nanostructures grown on CC.

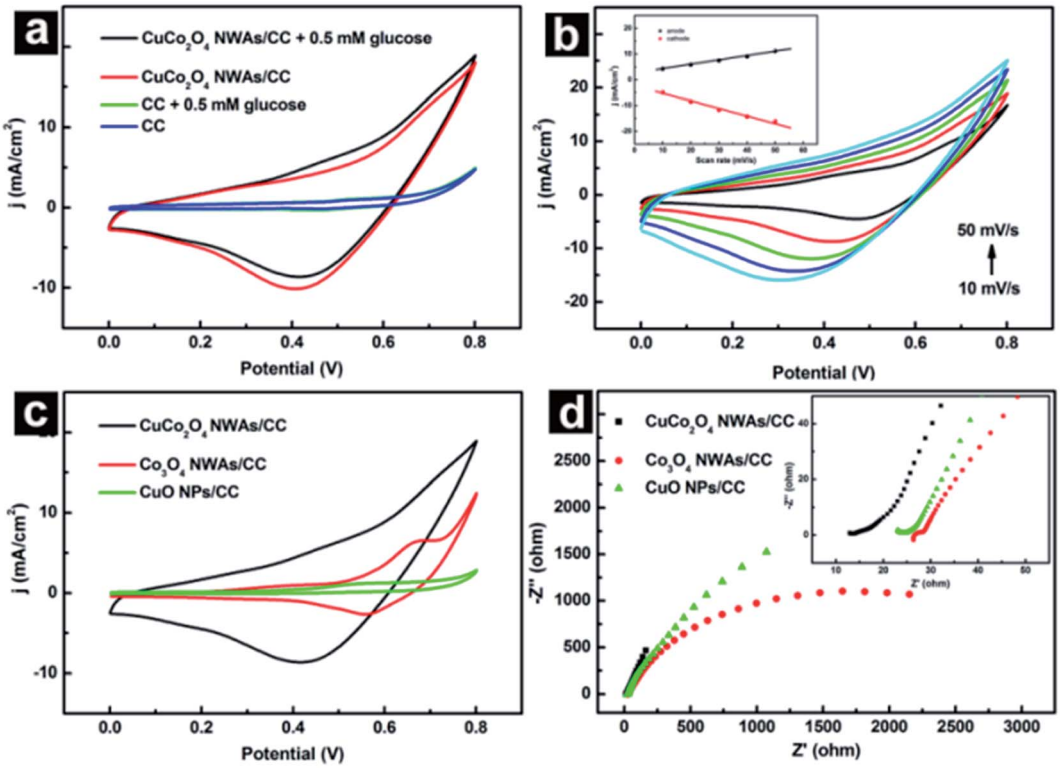

Fig. 4 (a) CVs of CC in the absence (blue curve) and presence (green curve) of 0.5 mM glucose, and $CuCo_2O_4$ NWAs/CC in the absence (red curve) and presence (black curve) of 0.5 mM glucose in 0.1 M NaOH solution with a scan rate of 20 mV s^{-1} (b) CVs of $CuCo_2O_4$ NWAs/CC in 0.1 M NaOH solution containing 0.5 mM glucose at various scan rates of 10, 20, 30, 40, 50 mV s^{-1}. Inset: the corresponding plots of current density *vs.* the scan rate. (c) CVs of $CuCo_2O_4$ NWAs/CC, Co_3O_4 NWAs/CC and CuO NPs/CC in 0.1 M NaOH solution containing 0.5 mM glucose with a scan rate of 20 mV s^{-1} (d) EIS results of $CuCo_2O_4$ NWAs/CC, Co_3O_4 NWAs/CC and CuO NPs/CC electrodes in 0.1 M NaOH solution. Inset is the amplifier region.

Cu based glucose enzyme-free sensor,[20,34,35] the oxidative current of Cu(II) to Cu(III) positioned at around 0.4 V was not obvious in the $CuCo_2O_4$ NWAs, which was agreed well with that of CuO NPs/CC in alkaline solution (green curve in Fig. 4c). Therefore, oxidative peaks at 0.4 V and 0.6 V can be attributed to the Co(II)/Co(III) and Co(III)/Co(IV) transitions,[23] which can be confirmed by the electrochemical behavior of Co_3O_4 NWAs/CC (Fig. 4c). The broad redox peaks at around 0.42 V are obvious for bare $CuCo_2O_4$ NWAs/CC electrode in alkaline solution, which can be assigned to the Co(IV)/Co(III), Co(III)/Co(II) and Cu(III)/Cu(II) transitions associated with anions OH^-.[23] The introduction of 0.5 mM glucose (black curve in Fig. 4a) causes a notable increase in anodic peak current density at 0.50 V, followed a gradual decrease in cathodic peak current density at 0.52 V, indicating an irreversible electro-oxidation reaction occurred at approximately around 0.50 V during electrochemical scanning.[34] These observations suggest the efficiency of $CuCo_2O_4$ NWAs/CC towards glucose electrooxidation. The possible electrocatalytic mechanism can be expressed as followings:[23,36]

$$2CuCo_2O_4 + OH^- + H_2O \rightarrow CuOOH + 2CoOOH + e$$

$$CoOOH + OH^- \rightarrow CoO_2 + H_2O + e$$

$$CoO_2 + \text{glucose} \rightarrow CoOOH + \text{gluconolactone}$$

$$CoOOH + \text{glucose} \rightarrow Co(OH)_2 + \text{gluconolactone}$$

$$CuOOH + \text{glucose} \rightarrow Cu(OH)_2 + \text{gluconolactone}$$

The kinetics of glucose oxidation on $CuCo_2O_4$ NWAs/CC electrode was examined by studying cyclic voltammograms (CVs) at different scan rates in 0.1 M NaOH solution containing 0.5 mM glucose. As shown in Fig. 4b and inset, both anodic and cathodic peak current densities exhibit good linear relationship with the scan rate within the range of 10–50 mV s^{-1}, indicating a surface-controlled process of glucose oxidation on the $CuCo_2O_4$ NWAs/CC electrode.

Here, we compared electrochemical behavior of $CuCo_2O_4$ NWAs/CC, Co_3O_4 nanowire arrays supported on CC (Co_3O_4 NWAs/CC) and CuO nanoparticles grown on CC (CuO NPs/CC). Fig. 4c shows CVs of $CuCo_2O_4$ NWAs/CC, Co_3O_4 NWAs/CC and CuO NP/CC in 0.1 M NaOH solution containing 0.5 mM glucose with a scan rate of 20 mV s^{-1}. A weak anodic peak at 0.50 V was observed on CuO NPs/CC, a larger anodic peak on Co_3O_4 NWAs/CC, while the largest redox peak on $CuCo_2O_4$ NWAs/CC electrode, indicative of the highest catalytic activity of $CuCo_2O_4$ NWAs/CC towards glucose. We further examined electrochemical impedance spectrum (EIS) of these electrodes to

evaluate their electron transfer activity. Fig. 4d shows EIS results of $CuCo_2O_4$ NWAs/CC, Co_3O_4 NWAs/CC and CuO NPs/CC electrodes in 0.1 M NaOH solution. In the low-frequency region, $CuCo_2O_4$ NWAs/CC shows a more ideal straight line, suggesting a more efficient electrolyte and proton diffusion. Moreover, the amplifier region in inset clearly shows that $CuCo_2O_4$ NWAs/CC has a lowest series resistance (13.8 Ω) among these electrodes. All these results demonstrated the enhanced electron conductivity of $CuCo_2O_4$ NWAs/CC and improved catalytic activity towards glucose, which should be attributed to the synergetic effect provided by copper and cobalt ions in $CuCo_2O_4$ spinal structures.

Since the applied potential has a significant effect on the response of an electrochemical sensor, it is of great importance to choose the optimal working potential. Fig. 5 shows amperometric responses of $CuCo_2O_4$ NWAs/CC to successive addition of 10 μM glucose into 0.1 M NaOH solution at different potentials. Obviously, the steady-state current response of 10 μM glucose increased rapidly from 0.45 to 0.55 V, and then gradually decreased from 0.55 to 0.60 V. Therefore, 0.55 V was chosen as the optimum applied potential for glucose detection, and the followed amperometric detection of glucose was performed under this potential.

Fig. 6a shows amperometric response of $CuCo_2O_4$ NWAs/CC with successive addition of the glucose solution with different concentrations into 0.1 M NaOH solution, at an applied potential of 0.55 V. The addition of glucose was incremented at the rate of 1, 5, 10, 50, and 100 μM, respectively. The successive additions of glucose caused a stepped increase in the anodic peak current. Inset shows the amplified response curve of $CuCo_2O_4$ NWAs/CC in a low glucose concentration indicated by a rectangle in Fig. 6a. As shown, the response increases immediately and reaches 95% of the steady state value within 5 s, suggesting a fast amperometric response behavior. The calibration curves of the oxidative current density *versus* glucose concentration are plotted in Fig. 6b. The linear regression is j (mA cm^{-2}) = 3.93C (mM) + 0.1095 (R^2 = 0.998). $CuCo_2O_4$ NWAs/CC displays a linear range from 1 μM to 0.93 mM, with

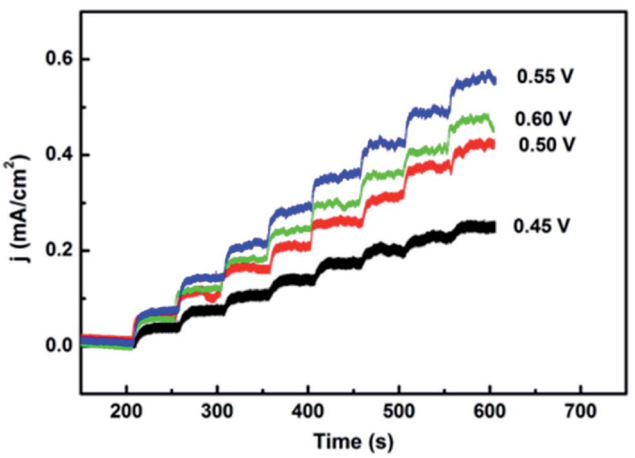

Fig. 5 Amperometric response with successive addition of 10 μM glucose at different potentials.

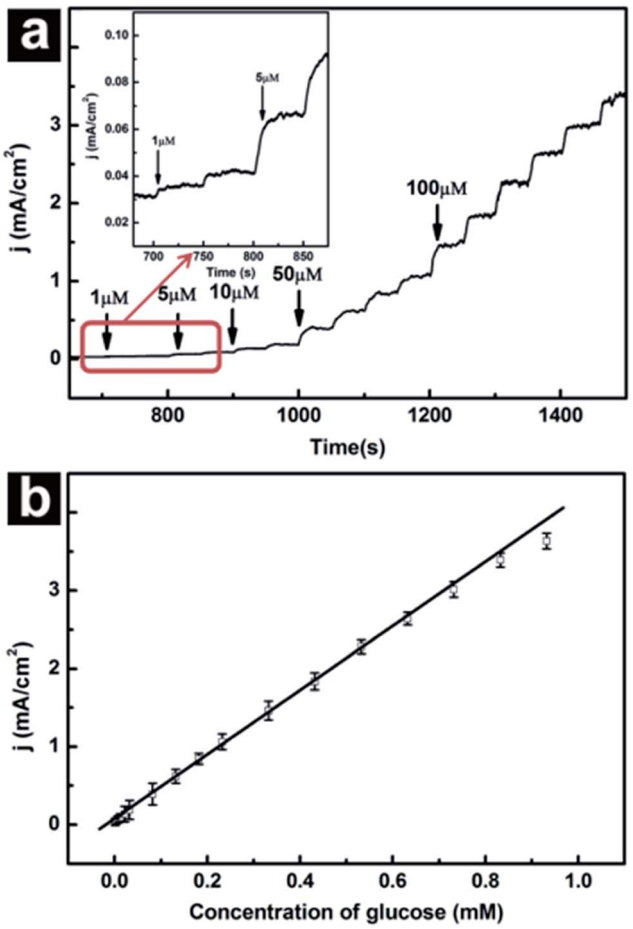

Fig. 6 (a) Amperometric response of $CuCo_2O_4$ NWAs/CC with successive addition of the glucose solution with different concentrations in to 0.1 M NaOH solution. Inset shows the amplified response curve of $CuCo_2O_4$ NWAs/CC in a low glucose concentration indicated by a rectangle. (b) Calibration curve for current density *vs.* concentration of glucose.

a sensitivity of 3.93 mA mM^{-1} cm^{-2} and a detection limit of 0.5 μM (S/N = 3). Such sensitivity is better than those of Cu based nanomaterial, such as 0.408 mA mM^{-1} cm^{-2} of Cu/CuO/ZnO hybrid hierarchical nanostructures,[37] 0.418 mA mM^{-1} cm^{-2} of $Cu(OH)_2$ nanotubes array,[38] 1.42 mA mM^{-1} cm^{-2} of hyperbranched Cu@Cu_2O coaxial nanowires mesh electrode,[39] 1.065 mA mM^{-1} cm^{-2} of CuO/graphene nanocomposites,[40] and so on. Moreover, such sensitivity is also comparable to the that of other Co based nanostructures like 0.526 mA mM^{-1} cm^{-2} of porous CoOOH nanosheet array,[41] 2.60 mA mM^{-1} cm^{-2} of ultrafine Co_3O_4 nanocrystals embedded carbon matrics,[21] 0.46 mA mM^{-1} cm^{-2} of Co_3O_4/PbO_2 core–shell nanorod array,[42] and 0.471 mA mM^{-1} cm^{-2} of 3D hierarchical porous cobalt oxide,[43] *etc.* (Table 1). Compared with the reported $CuCo_2O_4$ nanosheet electrode,[11,23] the present sensor still displays more favorable performance including higher sensitivity,[11] wider linear ranger,[11,23] and lower detection limit.[11,23] Such higher performance of $CuCo_2O_4$ NWAs/CC can be attributed to the following reasons: (1) the synergetic effect of copper and cobalt offers $CuCo_2O_4$ higher electron conductivity and electrochemical

Table 1 Analytical performances of $CuCo_2O_4$ NWAs/CC and other copper and cobalt based non-enzymatic glucose sensors

Electrode	Applied potential (V)	Sensitivity (mA mM^{-1} cm^{-2})	Linear range (mM)	Detection limit (μM)	Reference
Cu/CuO/ZnO hybrid hierarchical nanostructures	0.50	0.408	0.1 to 1	18	37
$Cu(OH)_2$ nanotube arrays	0.4	0.418	Up to 3	0.5	38
Hyper-branched Cu@Cu_2O coaxial nanowires	0.6	1.42	0.0007 to 2	0.04	39
CuO/graphene nanocomposites	0.6	1.065	0.001 to 8	1	40
CoOOH nanosheet array	0.52	0.526	0.003 to 1.109	1.37	41
Co_3O_4 nanocrystals embedded carbon matrics	0.55	2.60	0.01 to 0.8	1.0	21
Co_3O_4/PbO_2 core–shell nanorod array	0.55	0.46	0.005 to 1.2	0.31	42
3D hierarchical porous cobalt oxide	0.59	0.471	0.001 to 0.3	0.1	43
$CuCo_2O_4$ nanosheet on graphite paper	0.6	3.625	Up to 0.32	5	11
$CuCo_2O_4$ nanosheet on ITO	0.3	8.25	0.005 to 0.11	5.2	23
$CuCo_2O_4$ NWAs/CC	0.55	3.93	0.001 to 0.93	0.5	This work

activity. (2) 3D CC as conductive substrate facilitates more catalyst loading and more active site exposure. (3) The direct growth of $CuCo_2O_4$ NWAs on CC avoids the use of polymer binder, ensuring intimate contact and excellent electrical connection between them.[30] (4) 1D nanowire array structure of $CuCo_2O_4$ is known to be beneficial for the electronic conduction along the axial direction from the arrays to their substrate.

Selectivity is another major parameter for the practical use of glucose sensors, so it is important to perform anti-interference analysis. Dopamine (DA), ascorbic acid (AA), and uric acid (UA)

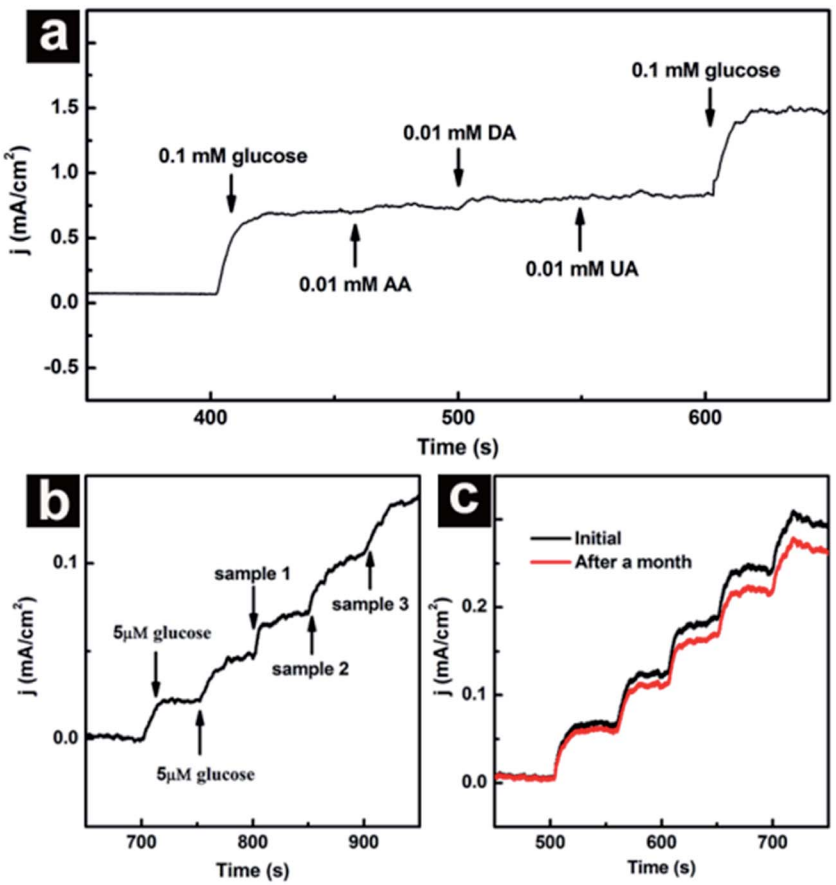

Fig. 7 (a) Amperometric response of $CuCo_2O_4$ NWAs/CC upon addition of successive addition of 0.1 mM glucose, 0.01 mM UA, 0.01 mM DA, 0.01 mM AA and 0.1 mM glucose at an applied potential of 0.55 V in 0.1 M NaOH solution. (b) Amperometric response upon addition of 5 μM glucose and three serum samples at an applied potential of 0.55 V in 0.1 M NaOH solution. (c) Amperometric response of $CuCo_2O_4$ NWAs/CC electrode towards 0.01 mM glucose initially and after a month.

Table 2 Glucose concentration in human serum samples that obtained in the hospital and those obtained by the $CuCo_2O_4$ NWAs/CC electrode

Sample	Glucose concentration obtained from the hospital (mM)	Glucose concentration obtained from the present sensor (mM)	RSD (%)	Bias (mM)
1	5.34	5.21	2.64	−0.13
2	6.26	6.35	2.33	0.09
3	6.47	6.52	1.26	0.05

have similar electroactive behavior to glucose and usually coexist with glucose in human samples. We thus evaluated the anti-interference performance of $CuCo_2O_4$ NWAs/CC towards these interfering species. Fig. 7a shows the amperometric responses of $CuCo_2O_4$ NWAs/CC electrode at 0.55 V in 0.1 M NaOH with successive addition of 0.1 mM glucose, 0.01 mM UA, 0.01 mM DA, 0.01 mM AA and 0.1 mM glucose. Note that the normal physiological level of glucose (3–8 mM) is more than 10 times higher than those of the other three interfering species,[44] the molar ratio of 10 : 1 was thus used for glucose and interferences to estimate their interference effects on the glucose sensing. As observed in Fig. 7a, $CuCo_2O_4$ NWAs/CC has remarkable response for glucose but negligible response for interfering species and the current density increases again with another addition of 0.1 mM glucose. These results demonstrate the superior selectivity of $CuCo_2O_4$ NWAs/CC against common interferences in glucose sensing.

To verify its feasibility for routine analysis, we further evaluated the reliability of the $CuCo_2O_4$ NWAs/CC electrode by detecting the glucose in human serum samples. All human serum samples were friendly supplied by Chongqing Emergency Medical Central. Fig. 7b shows the amperometric responses of the $CuCo_2O_4$ NWAs/CC electrode with addition of 5 μM glucose and three human serum samples at an applied potential of 0.55 V in 0.1 M NaOH solution. The determination of each sample was done three times to verify the reproducibility of the values. The concentration of glucose was determined by comparing the amperometric response of 5 μM glucose and that of human serum sample. Table 2 lists the glucose concentrations in serum samples obtained by the $CuCo_2O_4$ NWAs/CC electrode and those measured by the hospital. The relative standard deviations (RSD) and bias are less than 3% and 0.13 mM, respectively. These observations indicate that $CuCo_2O_4$ NWAs/CC electrode is suitable for practical sample testing.

The reproducibility and stability of the $CuCo_2O_4$ NWAs/CC electrode was also examined in our experiments. The reproducibility can be obtained by measuring the current response towards 0.01 mM glucose in 0.1 M NaOH solution at the $CuCo_2O_4$ NWAs/CC electrode. The relative standard deviation (RSD) of five parallel experiments was found to be 2.58%, suggesting reproducibility for glucose sensing. Additional, the above-mentioned results obtained from human samples (Table 2) also confirm the good reproducibility of present sensor. The long-term stability of the $CuCo_2O_4$ NWAs/CC electrode was evaluated by comparing the amperometric response towards 0.01 mM glucose in 0.1 M NaOH solution before and after a month. As observed Fig. 7c, the current response was found maintained 87% of the original value after a month conservation at room temperature, implying the good long-term stability of the present sensor.

Conclusions

$CuCo_2O_4$ NWAs/CC was fabricated *via* simple hydrothermal with subsequent annealing process. As a binary metal oxide based 3D nanowire arrays bind-free electrode, $CuCo_2O_4$ NWAs/CC has been proved as an efficient catalyst electrode for non-enzymatic glucose sensing under alkaline conditions. This electrode exhibits high performance towards glucose with a wide linear range, a low detection limit, a high sensitivity and selectivity, as well as good reproducibility and long-term stability.

Acknowledgements

This work was supported by the Natural Science Foundation of China (Grant No. 21601022), Foundation and Cutting-edge Research Plan of Chongqing (cstc2015jcyjA90002), and Project of International Science and Technology Cooperation Base Construction in Chongqing (cstc2014gjhz20002).

Notes and references

1 V. Scognamiglio, *Biosens. Bioelectron.*, 2013, **47**, 12–25.
2 C. Chen, Q. Xie, D. Yang, H. Xiao, Y. Fu, Y. Tan and S. Yao, *RSC Adv.*, 2013, **3**, 4473–4491.
3 S. A. Zaidi and J. H. Shin, *Talanta*, 2016, **149**, 30–42.
4 G. Rocchitta, O. Secchi, M. D. Alvau, D. Farina, G. Bazzu, G. Calia, R. Migheli, M. S. Desole, R. D. O'Neill and P. A. Serra, *Anal. Chem.*, 2013, **85**, 10282–10288.
5 A. J. Saleh Ahammad, A. Al Mamun, T. Akter, M. A. Mamun, S. Faraezi and F. Z. Monira, *J. Solid State Electrochem.*, 2016, **20**, 1933–1939.
6 A. L. Rinaldi and R. Carballo, *Sens. Actuators, B*, 2016, **228**, 43–52.
7 H. M. Jia, G. Chang, M. Lei, H. P. He, X. Liu, H. H. Shu, T. T. Xia, J. Su and Y. B. He, *Appl. Surf. Sci.*, 2016, **384**, 58–64.
8 K. C. Lin, C. Y. Yang and S. M. Chen, *Int. J. Electrochem. Sci.*, 2015, **10**, 3726–3737.
9 X. Chen, G. Li, G. Zhang, K. Hou, H. Pan and M. Du, *Mater. Sci. Eng., C*, 2016, **62**, 323–328.
10 B. Singh, N. Bhardwaj, V. K. Jain and V. Bhatia, *Sens. Actuators, A*, 2014, **220**, 126–133.

11 S. Liu, K. S. Hui and K. N. Hui, *ACS Appl. Mater. Interfaces*, 2016, **8**, 3258–3267.
12 L. Bie, X. Luo, Q. He, D. He, Y. Liu and P. Jiang, *RSC Adv.*, 2016, **6**, 95740–95746.
13 L. Kang, D. He, L. Bie and P. Jiang, *Sens. Actuators, B*, 2015, **220**, 888–894.
14 R. Madhu, V. Veeramani, S. M. Chen, A. Manikandan, A. Y. Lo and Y. L. Chueh, *ACS Appl. Mater. Interfaces*, 2015, **7**, 15812–15820.
15 S. Kim, S. H. Lee, M. Cho and Y. Lee, *Biosens. Bioelectron.*, 2016, **85**, 587–595.
16 H. Nie, Z. Yao, X. Zhou, Z. Yang and S. Huang, *Biosens. Bioelectron.*, 2011, **30**, 28–34.
17 A. Zhao, Z. Zhang, P. Zhang, S. Xiao, L. Wang, Y. Dong, H. Yuan, P. Li, Y. Sun, X. Jiang and F. Xiao, *Anal. Chim. Acta*, 2016, **938**, 63–71.
18 J. Yang, X. Liang, L. Cui, H. Liu, J. Xie, W. Liu and J. Yang, *Biosens. Bioelectron.*, 2016, **80**, 171–174.
19 S. Sun, X. Zhang, Y. Sun, S. Yang, X. Song and Z. Yang, *Phys. Chem. Chem. Phys.*, 2013, **15**, 10904–10913.
20 S. Sun, Y. Sun, A. Chen, X. Zhang and Z. Yang, *Analyst*, 2015, **140**, 5205–5215.
21 M. Li, C. Han, Y. Zhang, X. Bo and L. Guo, *Anal. Chim. Acta*, 2015, **861**, 25–35.
22 J. Jia, X. Li and G. Chen, *Electrochim. Acta*, 2010, **55**, 8197–8206.
23 K. K. Naik, S. Sahoo and C. S. Rout, *Microporous Mesoporous Mater.*, 2016, 1–9.
24 M. García, P. Batalla and A. Escarpa, *TrAC, Trends Anal. Chem.*, 2014, **57**, 6–22.
25 M. García, J. R. Alonso-Fernández and A. Escarpa, *Anal. Chem.*, 2013, **85**, 9116–9125.
26 M. García and A. Escarpa, *Biosens. Bioelectron.*, 2011, **26**, 2527–2533.
27 M. García, L. García-Carmona and A. Escarpa, *Microchim. Acta*, 2015, **182**, 745–752.
28 Z. Pu, Q. Liu, A. M. Asiri and X. Sun, *ACS Appl. Mater. Interfaces*, 2014, **6**, 21874–21879.
29 J. Tian, Q. Liu, A. M. Asiri and X. Sun, *J. Am. Chem. Soc.*, 2014, **136**, 7587–7590.
30 Z. Xing, Q. Liu, W. Xing, A. M. Asiri and X. Sun, *ChemSusChem*, 2015, **8**, 1850–1855.
31 Y. Luo, J. Jiang, W. Zhou, H. Yang, J. Luo, X. Qi, H. Zhang, Y. W. Denis, C. M. Li and T. Yu, *J. Mater. Chem.*, 2012, **22**, 8634–8640.
32 J. D. Roy-Mayhew, G. Boschloo, A. Hagfeldt and I. A. Aksay, *ACS Appl. Mater. Interfaces*, 2012, **4**, 2794–2800.
33 A. Shanmugavani and R. Kalai Selven, *Electrochim. Acta*, 2016, **188**, 852–862.
34 X. Niu, Y. Li, J. Tang, Y. Hu, H. Zhao and M. Lan, *Biosens. Bioelectron.*, 2014, **51**, 22–28.
35 K. Li, G. Fan, L. Yang and F. Li, *Sens. Actuators, B*, 2014, **199**, 175–182.
36 X. Dong, H. Xu, X. Wang, Y. Huang, M. B. Chan-Park, H. Zhang, L. H. Wang, W. Huang and P. Chen, *ACS Nano*, 2012, **6**, 3206–3213.
37 S. SoYoon, A. Ramadoss, B. Saravanakumar and S. J. Kim, *J. Electroanal. Chem.*, 2014, **717–718**, 90–95.
38 S. Zhou, X. Feng, H. Shi, J. Chen, F. Zhang and W. Song, *Sens. Actuators, B*, 2013, **177**, 445–452.
39 Y. Zhao, L. Fan, Y. Zhang, H. Zhao, X. Li, Y. Li, L. Wen, Z. Yan and Z. Huo, *ACS Appl. Mater. Interfaces*, 2015, **7**, 16802–16812.
40 Y. W. Hsu, T. K. Hsu, C. L. Sun, Y. T. Nien, N. W. Pu and M. D. Ger, *Electrochim. Acta*, 2012, **82**, 152–157.
41 L. Zhang, C. Yang, G. Zhao, J. Mu and Y. Wang, *Sens. Actuators, B*, 2015, **210**, 190–196.
42 T. Chen, X. Li, C. Qiu, W. Zhu, H. Ma, S. Chen and O. Meng, *Biosens. Bioelectron.*, 2014, **53**, 200–206.
43 L. Han, D. P. Yang and A. Liu, *Biosens. Bioelectron.*, 2015, **63**, 145–152.
44 E. Scavetta, B. Ballarin and D. Tonelli, *Electroanalysis*, 2010, **22**, 427–432.